Microchemical Journal 141 (2018) 240–246

Contents lists available at ScienceDirect

Microchemical Journal

journal homepage: www.elsevier.com/locate/microc

Analytical applications of Cu@PtPd/C nanoparticles for the quantification of hydrogen peroxide

F.A. Gutierrez[a,*], I.S. Giordana[a], V.C. Fuertes[a], A.E. Montemerlo[a], J.M. Sieben[b], A.E. Alvarez[b], M.D. Rubianes[a,*], G.A. Rivas[a,*]

[a] INFIQC, Facultad de Ciencias Químicas, Universidad Nacional de Córdoba, Haya de la Torre S/N, Ciudad Universitaria, 5000 Córdoba, Argentina
[b] Instituto de Ingeniería Electroquímica y Corrosión and CONICET, Universidad Nacional del Sur, B8000CPB Bahía Blanca, Argentina

ARTICLE INFO

Keywords:
Electrochemical sensor
Core-shell nanoparticles
Platinum
Palladium
Copper
Hydrogen peroxide sensor
Cu@PtPd/C

ABSTRACT

This work reports a non-enzymatic amperometric sensor for hydrogen peroxide based on the use of a glassy carbon composite electrode modified with core-shell Cu@PtPd/C nanoparticles. Cu@PtPd/C presents an important electrocatalytic activity towards hydrogen peroxide reduction. The comparison of the sensitivities and the charge transfer resistances for hydrogen peroxide at the glassy carbon composite electrode modified with 5.0% w/w Pt/C, Pd/C, Pd/C + Pt/C and Cu@PtPd/C demonstrate a clear synergism on the catalytic reduction of hydrogen peroxide at −0.100 V when having Pt, Pd and Cu incorporated in the core-shell nanostructure. The best compromise between sensitivity, reproducibility and response time was reached with 20.0% w/w Cu@PtPd/C. For the selected sensor (glassy carbon composite electrode containing 20.0% w/w GCPE/Cu@PtPd/C) the analytical parameters are highly competitive compared to similar devices reported in the last years, with a linear relationship between current and hydrogen peroxide concentration between 5.0×10^{-6} and 2.5×10^{-4} M, sensitivity of $(5.30 \pm 0.09) \times 10^{5}$ μAM^{-1} cm^{-2} ($r^2 = 0.998$) and detection limit of $(3.7 \pm 0.5) \times 10^{-7}$ M. The resulting sensing platform was successfully used for the quantification of hydrogen peroxide in a mouth-wash sample.

1. Introduction

Hydrogen peroxide is a compound of great importance in diverse fields. In fact, it is a by-product of different metabolic routes mainly connected with the action of oxidases [1,2]. Due to their oxidative properties, hydrogen peroxide has been widely used for the synthesis of organic compounds, pulp and paper bleaching, sterilization and clinical applications [6,7]. High levels of this compound may produce diseases connected with oxidative stress like cancer, cardiovascular disorders and Alzheimer disease [3–5]. Therefore, even when several methodologies have been proposed for the quantification of hydrogen peroxide [8], the development of new analytical platforms that allows the efficient quantification of hydrogen peroxide is highly required.

Electrochemical sensing methods have been successfully used due to their known advantages connected with low cost, simple operation, high sensitivity, easy miniaturization and automation [9]. One important group of hydrogen peroxide electrochemical sensors is based on the use of heme-proteins like peroxidase, cytochrome, catalase and myoglobin [10–13]. Although these sensors represent a very interesting alternative for the quantification of hydrogen peroxide, they have some drawbacks associated with the cost and instability of the enzymes. Consequently, there is increasing interest in developing non-enzymatic strategies for the quantification of hydrogen peroxide [14,15]. Many of them have been based on the electrocatalytic activity of metallic particles [16–31]. The modification of carbon electrodes with rhodium, copper, platinum, palladium, gold and combination of these metals [16,25]; metal oxides [26–29]; perovskites [30] and magnetite [31] has demonstrated to be highly successful for the low-potential detection of hydrogen peroxide.

With the advent of Nanotechnology, the development of nanosized electrocatalysts-based sensors for hydrogen peroxide have received enormous attention due to the known advantages of nanomaterials attributed to their quantum size effect, excellent conductivity and biocompatibility [32]. Among nanomaterials, core-shell nanostructures present important advantages compared to their monometallic counterparts related to the stability, dispersability, surface modification, catalytic activity and possibility to tune their physical and chemical properties just by varying the composition and arrangement of atoms and size of the clusters [33,34].

In this work we report for the first time the electrocatalytic activity

* Corresponding authors.
E-mail address: grivas@fcq.unc.edu.ar (G.A. Rivas).

https://doi.org/10.1016/j.microc.2018.05.019
Received 21 February 2018; Received in revised form 23 April 2018; Accepted 12 May 2018
Available online 17 May 2018
0026-265X/

of Cu@PtPd/C core-shell nanoparticles towards the reduction of hydrogen peroxide and the development of a glassy carbon composite (paste) electrode (GCPE) modified with these nanostructures for the amperometric quantification of this important analyte. In the following sections we present: i) a critical discussion about the influence of the amount of core-shell nanoparticles on the amperometric and impedimetric response of the resulting sensors towards the reduction of hydrogen peroxide; ii) a comparison of the analytical performance of GCPEs modified with Cu@PtPd/C, individual nanoparticles (Pt/C or Pd/C) or the physical mixture of Pt/C and Pd/C and iii) the application of the proposed sensor for the quantification of hydrogen peroxide in a real sample.

2. Experimental section

2.1. Reagents

Hydrogen peroxide (30% v/v aqueous solution) and mineral oil were purchased from Baker. Glassy carbon powder and Vulcan XC-72 R carbon black was obtained from Alfa Aesar and Cabot Corp. respectively. $CuSO_4$was received from Merck. $NaBH_4$ (> 94%), $H_2PtCl_6{\cdot}6H_2O$, $PdCl_2$, mineral oil, ascorbic acid (AA), uric acid (UA) and glucose oxidase (GOx type X-S, *Aspergillus niger*, EC 1.1.3.4., 157,500 Units per gram of solid, catalog number G-7141) were purchased from Sigma-Aldrich. All chemicals were reagent grade and used without further purification.

Cu@PtPd/C nanoparticles were synthesized according to the procedure described by Sieben et al. [35]. Briefly, copper nanoparticles supported on acid-treated Vulcan XC-72 R carbon black were synthesized by reduction of $CuSO_4$ with $NaBH_4$ in a citrate buffer solution at room temperature to obtain 60 wt% Cu in carbon. The Cu/C material was filtered, thoroughly washed with distilled water and ethanol and finally dried at 70 °C. The Cu@PtPd core-shell particles were prepared by galvanostatic displacement of Cu with Pt and Pd. $H_2PtCl_6{\cdot}6H_2O$ and $PdCl_2$ acidic aqueous solutions were added to Cu/C and left to react for 120 min under magnetic stirring. The solid product was filtered, washed with distilled water and ethanol and dried in oven overnight. The platinum, palladium and copper content in the as-prepared material was6.2, 2.2 and 0.7 wt%, respectively. For comparison, Pt/C and Pd/C materials with a noble metal content of 6.2 wt% were also prepared in a similar way.

Ultrapure water (ρ = 18 MΩcm) from a Millipore-MilliQ system was used for preparing all the solutions. A 0.050 M phosphate buffer solution pH 7.40 was employed as supporting electrolyte.

2.2. Procedure

The electrochemical measurements were performed with Epsilon (BAS), TEQ-04 and AUTOLAB (model PGSTAT100) potentiostats. The electrodes were inserted into the cell (BAS, Model MF-1084) through holes in its Teflon cover. A platinum wire and Ag/AgCl, 3 M KCl (BAS, Model RE-5B) were used as counter and reference electrodes, respectively. All potentials are referred to the latter. A magnetic stirrer provided the convective transport during the amperometric measurements.

The glassy carbon composite (paste) electrode (GCPE) was prepared in a regular way by mechanically mixing glassy carbon microspheres (90.0% w/w) and mineral oil (10.0% w/w) in an agate mortar for 30 min. GCPEs containing Cu@PtPd/C were prepared in a similar way, mixing first the Cu@PtPd/C nanoparticles with mineral oil for 5 min, followed by the incorporation of the glassy carbon microspheres and mixing for additional 30 min. GCPE/Pt/C and GCPE/Pd/C, were prepared by using Pt/C and Pd/C instead of the core-shell nanoparticles. GCPE was also modified with a physical mixture of Pt/C and Pd/C (GCPE/(Pt/C + Pd/C). In the case of GCPE modified with Cu@PtPd/C and GOx, the core-shell nanoparticles were first mixed with the mineral oil and GOx for 10 min, followed by the incorporation of the glassy carbon microspheres and additional mixing for 30 min. A portion of the given paste was packed firmly into a Teflon tube cavity (3 mm diameter). The electric contact was established through a stainless steel screw. The surface was smoothed on a weighing paper before starting every new experiment.

Amperometric measurements were conducted in a stirred 0.050 M phosphate buffer solution pH 7.40 by applying the desired working potential and allowing the transient currents to decay to a steady-state value prior to the addition of the analyte and subsequent current monitoring.

Electrochemical Impedance Spectroscopy (EIS) measurements were performed with an AUTOLAB model PGSTAT100 potentiostat. EIS experiments were performed in the frequency range between 10 KHz and 10 mHz, with a potential perturbation of 10 mV and a working potential of -0.100 V using 2.5×10^{-2} M hydrogen peroxide solution. The impedance spectra were analyzed by using the *Z*-view software. All measurements were performed at room temperature.

The structural characterization of the nanoparticles supported on the activated carbon powder was carried out by Powder X-Ray Diffraction (PXRD) data using a PAN alytical X'Pert PRO powder diffractometer (40 kV, 40 mA) in Bragg–Brentano reflection geometry with CuKα radiation (λ = 1.5418 Å).The data were obtained in the 2θ range between 30° and 85° in steps of 0.02° and a counting time of 5.2 s per step.The particle size distribution was determined by measuring the diameter of about 150 particles using the Image J analysis software. The particle size was determined using transmission electronic microscopy(TEM, JEOL, 100CX II) operated at 200 keV.

3. Results and discussion

3.1. Surface characterization of GCPE/Cu@PdPt/C

Fig. 1A depicts a typical TEM image of Cu@PtPd/C nanoparticles. The micrography reveals the presence of a large amount of almost rounded nanoparticles of (2.9 ± 0.4) nm diameter regularly distributed on the carbon material. The inset shows the particle size distribution obtained from the diameter of about 150 nanoparticles using the Image J analysis software. This average size presents very good agreement with the value calculated using the Scherrer's equation. The average of the nanoparticles size for the four different batches used here was 3.1, 3.2, 3.0 and 2.9 nm.

Fig. 1B displays the XRD patterns for Pd/C (a), Pt/C (b) and Cu@PtPd/C (c). Four diffraction peaks are shown at Bragg angles of approximately 40, 46, 68 and 82°, which can be assigned to (111), (200), (220) and (311) crystal planes of a face centered cubic (*fcc*) structure [36]. No peaks for Cu were observed in the XRD spectrum of Cu@PtPd/C system, suggesting that the nanoparticles are composed of a Cu-rich core surrounded by a PtPd alloy shell. Similar behavior has been observed in the case of PdCu@Pt [37] and Au@Ag [38] core-shell nanoparticles. The diffraction peaks of Cu@PtPd/C show a slight shift towards higher 2θ values compared to Pd/C and Pt/C, caused by the smaller interplanar spacing, due to the smaller atomic radius of Cu, effect that is more pronounced at higher angles. The refinement of the crystal structure, performed by the Rietveld method [39], showed a good agreement with the experimental data (data not shown). Refined cell parameters (*a*(Å)) demonstrated that the presence of Cu in the core generates a contraction in the cubic lattice parameter that produces a shifting of the d-band of Pt to lower energies [40,41] (see Table SI-1).

Fig. 1C,a shows the XRD spectra for GCPE modified with Cu@PtPd/C (20.0% w/w). This pattern presents diffraction peaks associated to the crystal planes of Pd and Pt superimposed on a major amorphous component of the mineral oil and glassy carbon of the composite. For comparison, the spectrum for GCPE is also included (Fig. 1C,b).

The atomic ratio of Pt:Pd:Cu in Cu@PdPt, determined by EDX, was 50.9:32.4:16.7 and the structural analysis revealed that the nanosized particles are composed of a Cu-rich core covered by a Pt—Pd rich shell.

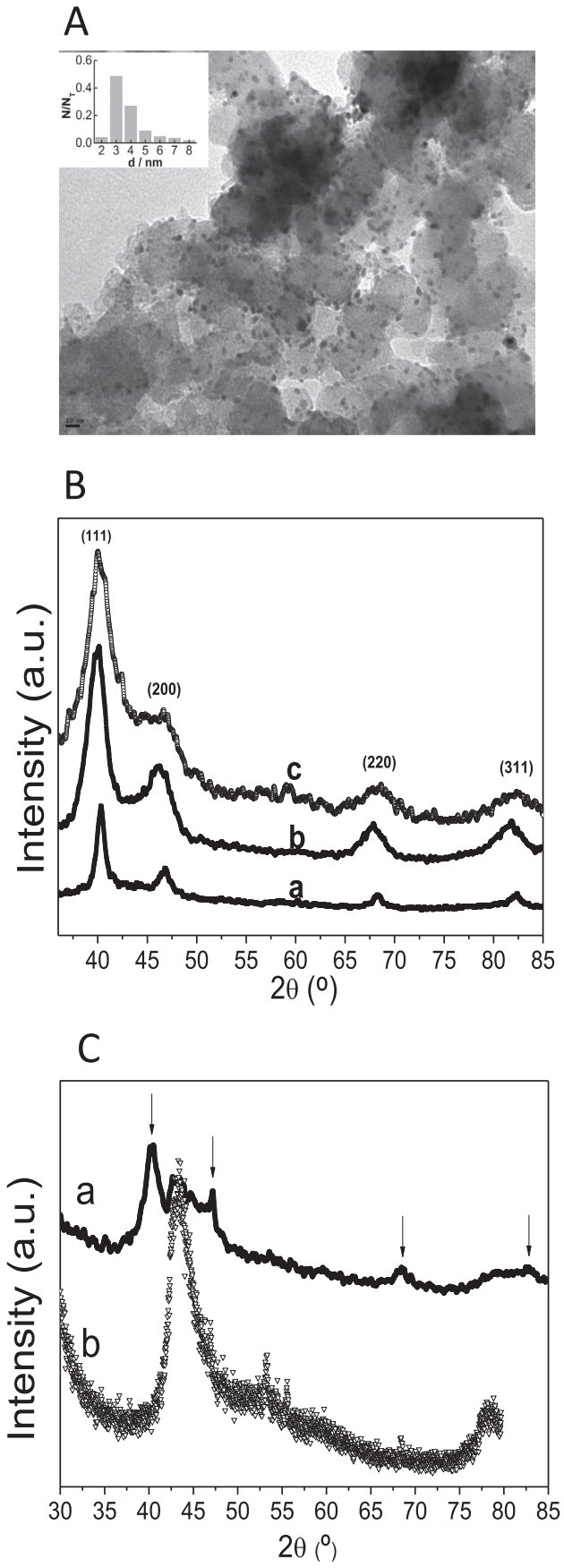

Fig. 1. (A)TEM image of Cu@Pt-Pd/C powder. The corresponding histogram of particle size distribution is displayed in the inset; (B) XRD patterns for Pd/C (a), Pt/C (b) and Cu@PdPt/C (c).(C) a) XRD pattern of GCPE modified with Cu@PdPt/C (20.0% w/w), b) XRD pattern of GCPE.

3.2. Electrochemical characterization of GCPE/Cu@PtPd/C

Fig. 2 depicts cyclic voltammograms for 0.050 M hydrogen peroxide obtained at GCPE (dashed line and inset) and GCPE containing 5.0% w/w Cu@PtPd/C (solid line). The voltammetric profiles show that the presence of the core-shell nanoparticles produces a decrease in the overvoltages for oxidation and reduction of hydrogen peroxide (130 and 175 mV, respectively) and a huge enhancement in the currents associated with both processes, evidencing a clear electrocatalytic effect of Cu@PdPt/C towards the reduction and oxidation of hydrogen peroxide. No significant changes were observed in the voltammetric profiles performed in deoxygenated solutions, indicating that there is no interference due to the reduction of oxygen.

To evaluate the advantages of the core-shell nanoparticles on the catalytic activity towards the reduction of hydrogen peroxide compared to the monometallic counterparts and physical mixture of them, we performed amperometric experiments at −0.100 V using different electrodes. Fig. 3A shows the sensitivities for hydrogen peroxide reduction obtained from amperometric experiments at (a) GCPE and GCPE modified with 5.0 % w/w of Pd/C (GCPE/Pd/C), Pt/C (GCPE/Pt/C), the mixture of Pt/C and Pd/C (GCPE/(Pt/C + Pd/C)) and Cu@PtPd/C (GCPE/Cu@PtPd/C) (see also Table SI-2). Compared to GCPE, the sensitivity increases when GCPE is modified either with Pd/C (4 times), Pt/C (14 times), Pd/C + Pt/C (25 times) or Cu@PdPt/C (100 times). This important enhancement in the sensitivity for the reduction of hydrogen peroxide observed at GCPE modified with Cu@PtPd/C clearly demonstrate a synergic effect of Pd and Pt nanoparticles deposited onto the core of Cu. This synergism can be attributed to the lattice strain produced by the core of Cu that originate changes in the electronic structure of Pt and, consequently, in the DOS at the Fermi level [40,41].

To obtain complementary information about the electrochemical behavior of GCPE/Cu@PtPd/C, the system was also evaluated by EIS. Fig. 3B displays the Nyquist plots obtained in a 2.5×10^{-2} M hydrogen peroxide solution at −0.100 V using bare GCPE (inset, a) and GCPE modified with 5.0% w/w of (b) Pd/C, (c) Pt/C, (d) Pd/C + Pt/C, and (e) Cu@PtPd/C. The experimental data (symbols) demonstrate a very good agreement with the equivalent circuit ($R_s(R_{ct}C_{dl})$) (solid lines), where R_{ct} is the charge transfer resistance, C_{dl} is the double layer capacitance, and R_s is the electrolyte resistance. As can be seen from the semi-circles at high frequencies, R_{ct} decreases when GCPE is modified either with the individual nanoparticles (Pd/C or Pt/C), the physical mixture of them (Pd/C + Pt/C) or the core-shell (Cu@PtPd/C) nanoparticles, the values being $(3.9 \pm 0.8) \times 10^7$, $(7.5 \pm 0.4) \times 10^5$, $(3.6 \pm 0.3) \times 10^5$, $(2.0 \pm 0.4) \times 10^5$ and $(5.5 \pm 0.8) \times 10^4 \Omega\,cm^{-2}$, for GCPE, GCPE/Pd/C, GCPE/Pt/C, GCPE/Pd/C + Pt/C and GCE/Cu@PtPd/C, respectively. The large decrease in R_{ct} observed for GCPE/Cu@PtPd/C compared to GCPE/Pd/C + Pt/C confirms the synergism of Cu@PtPd/C on the catalytic activity towards hydrogen peroxide electro-reduction, as it was previously demonstrated by amperometry, reinforcing the key role of Cu.

The amount of Cu@PtPd/C is an important parameter for the development of the sensor. Fig. 4A displays the effect of the amount of Cu@PtPd/C nanoparticles present in the composite on the sensitivity towards the reduction of hydrogen peroxide (obtained from amperometric experiments at −0.100 V). The sensitivity increases almost linearly with the amount of nanoparticles up to 20% w/w. Higher percentages of core-shell nanoparticles were also evaluated, although under these conditions, the reproducibility of the signal becomes poorer due to the lack of stability of the composite electrode. Fig. 4B depicts Nyquist plots obtained in a 2.5×10^{-2} M hydrogen peroxide solution at −0.100 V using bare GCPE (inset, a) and GCPE modified with(b) 2.5% w/w, (c) 5.0% w/w, (d) 7.5% w/w, (e) 10.0% w/w, (f) 12.5% w/w, (g) 15.0% w/w, and (h) 20.0% w/w Cu@PtPd/C. A very good correlation between the experimental data (symbols) and the model ($(R_s(R_{ct}C_{dl}))$, solid lines) is also observed here. The R_{ct} largely decreases

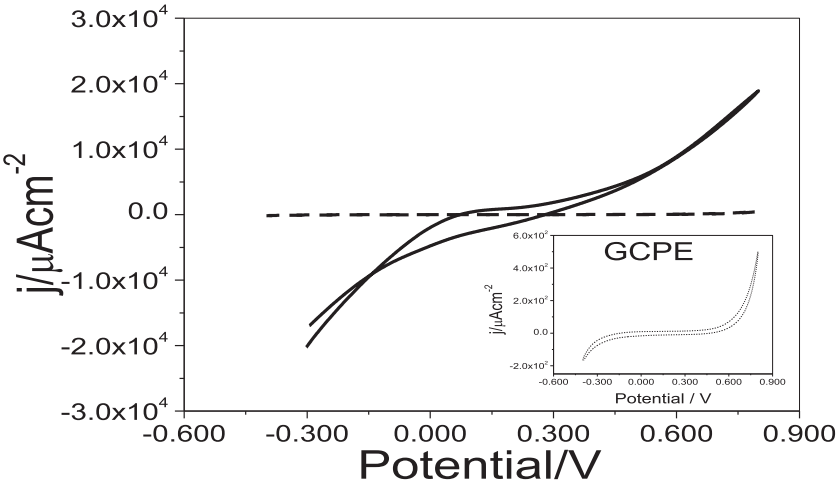

Fig. 2. Cyclic voltammograms for 0.050 M hydrogen peroxide at GCPE (dotted line and inset) and GCPE/Cu@PtPd/C5.0% w/w (solid line). Scan rate: 0.100 V·s^{-1}.

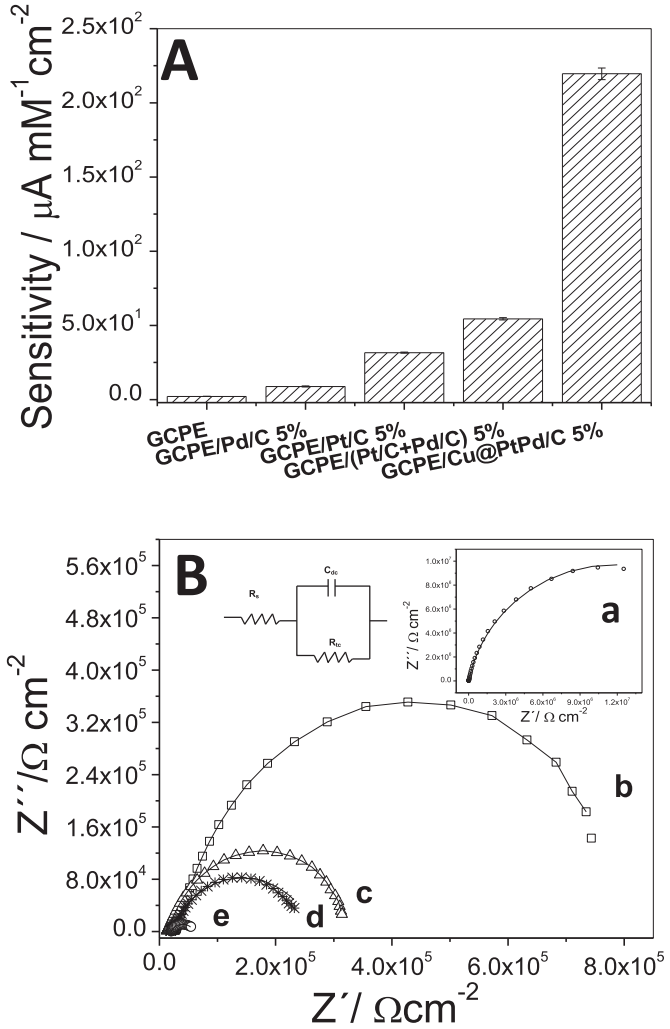

Fig. 3. (A) Variation of the sensitivity obtained from amperometric experiments for successive additions of hydrogen peroxide at −0.100 V (A) and Nyquist plots (B) obtained at GCPE (a inset) and GCPE containing 5.0% w/w of different nanomaterials: Pd/C (b), Pt/C (c), Pt/C + Pd/C (d) and Cu@PdPt/C (e). The insets of Fig. 3B display the equivalent circuit. Supporting electrolyte: 0.050 M phosphate buffer solution, pH 7.40.

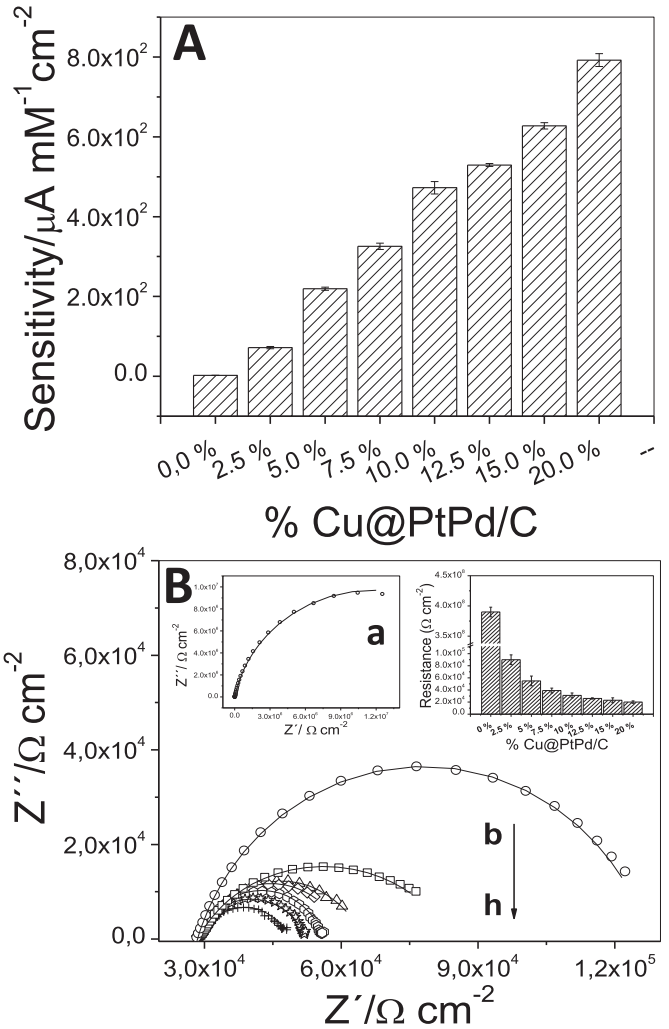

Fig. 4. (A) Variation of the sensitivity obtained from amperometric experiments for successive additions of hydrogen peroxide at −0.100 V at GCPE containing different amounts of Cu@PdPt/C: 0.0, 2.5, 5.0, 7.5, 10.0, 12.5, 15.0. 20.0 (% w/w). (B) Nyquist plots obtained for 0.050 M hydrogen peroxide at open circuit for −0.100 V at GCPE containing different amounts of Cu@PdPt/C: 0.0 (a, inset), 2.5 (b), 5.0 (c), 7.5 (d), 10.0 (e), 12.5 (f), 15.0 (g), 20.0 (h) % w/w. The inset shows the bar plots for the charge transfer resistances obtained at the different electrodes (a-h). Supporting electrolyte: 0.050 M phosphate buffersolution, pH 7.40.

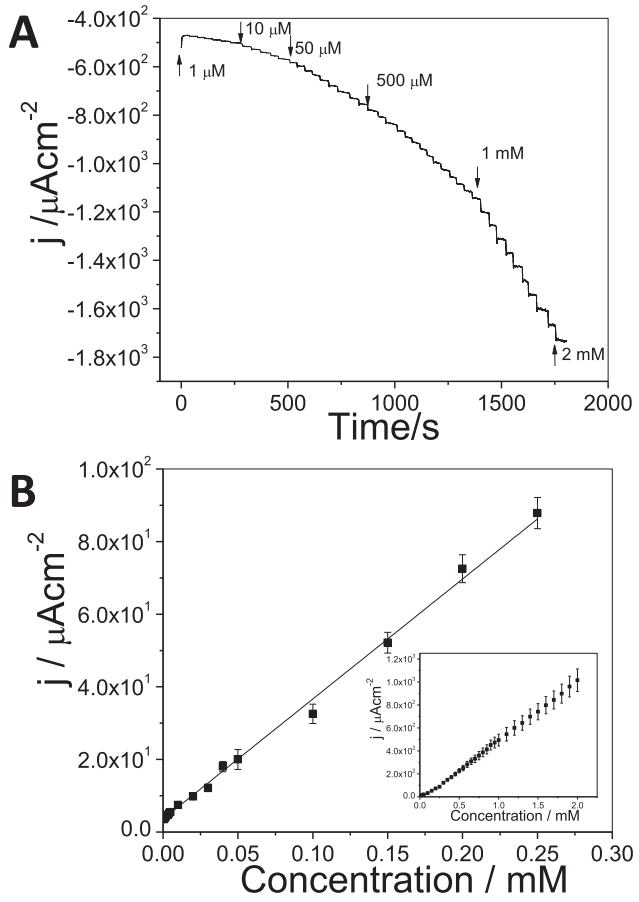

Fig. 5. (A) Amperometric recording obtained at GCPE/Cu@PdPt/C at −0.100 V for successive additions of hydrogen peroxide (as indicated in the figure). (B) Calibration plot obtained from the amperometric response at −0.100 V. The inset displays the calibration plot for a wide range of hydrogen peroxide concentrations (between 1.0×10^{-6} M and 2.0×10^{-3} M).

as the amount of core-shell nanoparticles increases (inset of Fig. 4B), in agreement with the results previously shown (Fig. 4A).

The important enhancement of sensitivity and the drastic decrease of R_{ct} for hydrogen peroxide reduction clearly demonstrate the key role of the amount of core-shell nanoparticles present in the composite electrode on the electrocatalytic activity. The selected percentage of Cu@Pt-Pd/C nanoparticles for further work was 20.0% (w/w) as the best compromise between signal-to-noise ratio, sensitivity, R_{ct}, stability of the signal and response time.

3.3. Analytical performance

Fig. 5A shows amperometric recordings for successive additions of hydrogen peroxide at GCPE/Cu@PtPd/C (20.0% w/w) obtained at −0.100 V. A fast and clear response is observed after each addition of hydrogen peroxide. The corresponding calibration plot is depicted in Fig. 5B. The analytical parameters are the following: linear range from 5.0×10^{-6} to 2.5×10^{-4} M; sensitivity: $(5.30 \pm 0.09) \times 10^{5}\,\mu A M^{-1}\,cm^{-2}$ ($r^2 = 0.998$), detection limit: $(3.7 \pm 0.5) \times 10^{-7}$ M (taken as 3 × σ/S, where σ is the standard deviation of the blank signal and S the sensitivity).

Table 1 summarizes the analytical parameters for the most relevant non-enzymatic hydrogen peroxide sensors based on the use of different metallic and core-shell nanoparticles reported since 2013. The comparison allowed us to conclude that our sensor presents better [42–52] or comparable [53–55] detection limits than most of the sensors, with very wide linear range and excellent sensitivity. The detection limits reported in [56–61] are better than the one informed in this work; however, our sensor presents the great advantage of easy preparation and a very simple transduction scheme at considerably less negative potentials. Some typical hydrogen peroxide electrochemical enzymatic sensors obtained by combination of peroxidase or proteins with peroxidase-like activity and nanomaterials presents, as in the case of our sensor, detection limits at the sub-μM level [62–65] with the exception of a glassy carbon electrode modified with heterostructured multi-walled carbon nanotubes and graphene oxide nanoribbons, chitosan and myoglobin that presents a detection limit at nM level [66] (Table SI-3). However, is important to remark that this biosensor presents a more complex preparation and involves expensive materials like myoglobin, multi-walled carbon nanotubes and graphene oxide nanoribbons, at variance with the simple preparation of our sensor that relies just on the mixing of the synthesized Cu@PtPd/Cwith glassy carbon microspheres and mineral oil.

The average sensitivity for hydrogen peroxide at GCPE-Cu@PtPd/C obtained from ten consecutive calibration plots was $(6 \pm 1) \times 10^{5}\,\mu A M^{-1}\,cm^{-2}$, demonstrating that the average sensitivity remained very close to the original one (fresh electrode), although the associated uncertainty increases up to 16.7% due to the random distribution of the sensitivities for the different calibration plots. The reproducibility of GCPE/Cu@PtPd/C using the same dispersion and 3 different electrodes was 3.8%. Amperometric experiments performed at −0.100 V with the same composite stored at room temperature, demonstrated an excellent long-term stability since after 18 months of storage the sensitivity was around 10% higher than the original one (probably due to the loss of mineral oil during the storage).

Considering further analytical applications of Cu@PtPd/C for developing oxidases-based enzymatic biosensors, we evaluated the possible interference of UA and AA by amperometry at −0.100 V (results not shown). No interference was obtained after addition of 5.0×10^{-6} M H_2O_2 followed by additions of 1.0×10^{-4} M AA and 4.0×10^{-4} M UA, demonstrating the advantages of the preferential electrocatalytic detection of hydrogen peroxide.

The analytical platform was challenged with a real sample, in this case, mouthwash, “Colgate Plax Whitening®”. The concentration obtained with our sensor was (1.38 ± 0.03) % w/v demonstrating very good agreement with the value reported in the product (1.5% w/v hydrogen peroxide as the active ingredient).

Some preliminary results about the incorporation of glucose oxidase (GOx) in the composite GCPE/Cu@PtPd/C demonstrated that the sensitivity for amperometric determinations of hydrogen peroxide at −0.100 V is 5 times higher than those obtained in the absence of the protein, indicating that, as in the case of other composite materials [67], the protein plays a very important role in the dispersion of the Cu@PtPd/C nanoparticles within the composite.

The results shown here demonstrate that the use of Cu@PtPd/C represents a very interesting avenue for improving the performance of hydrogen peroxide electrochemical (bio)sensors due to the excellent catalytic effect of the hybrid material.

4. Conclusions

We report for the first time the electrocatalytic activity of Cu@PtPd/C core-shell nanoparticles towards the reduction of hydrogen peroxide and the synergism of the three components (Cu, Pt and Pd) compared to the individual ones (Pt/C or Pd/C) or their physical mixture. The electrocatalytic activity of the core-shell nanoparticles has made possible the development of a very competitive, low-cost and easy-to-prepare amperometric hydrogen peroxide sensor with analytical parameters comparable to most of the recent non-enzymatic and enzymatic electrochemical hydrogen peroxide sensors. The high sensitivity excellent reproducibility, and successful application of the sensor for the quantification of hydrogen peroxide in a real sample make the proposed sensor an interesting alternative for further development of other (bio)

Table 1
Analytical characteristics of different non-enzymatic hydrogen peroxide electrochemical sensors.

Platform	Detection limit (μM)	Working potential (V)	Sensitivity ($\mu A\ mM^{-1}\ cm^{-2}$)	Linear range (μM)	Reference
Pd/PDDA/PG	0.9	−0.1	816.7	2–1672	[42]
Pt/PG/GCE	< 0.50	−0.1	341.14	1–1477	[43]
Ag@Pt–G/GCE	0.9	−0.35	–	5–12,400	[44]
Au@Ag/GCE	0.67	−0.54	–	2–7020	[45]
3D N-Co-CNT@NG	2.00	−0.04	28.66	2.0–7449	[46]
Pt0.5Au0.5@C	2.4	0.3	210.3	7.0–6500	[47]
Pt-IL-pGR-GCE	0.42	0.074	942.15	10 to 4000	[48]
Pd NP-Cu	2.1	1.2	–	100–2000	[49]
AuNPs@Gr/NiF	1	−0.2	47.4	50–1750	[50]
$CoWO_4$	10.7	0.2	–	< 24,900	[51]
$CuFe2O_4$/RGO/CPE	0.52	−0.350	–	2–200	[52]
Pt NP–Ni foam electrode	0.3	−0.05	829	5–850	[53]
Ag@Cu	0.3	−0.35	85.1	0.5–50	[54]
Graphene/pectin-CuNPs	0.35	−0.2	391	1.0–1000	[55]
GCE/Cu@Pt/C	0.15	−0.3	351.3	0.50–32,560	[56]
Au/PPG/CNT	0.017	−0.6	–	1–150	[57]
RGO/Pt-Ag	0.04	−0.05	699.6	5–1500	[58]
Au@C@Pt/GCE	0.13	0	144.7	9–1860	[59]
GO/Au@Pt@Au	0.25	−0.3	–	0.5–110,000	[60]
rGO/FeNPs nanocomposite	0.06	−0.5	208.5	0.1–2150	[61]
Cu@Pt-Pd/C	0.37	−0.100	530	5–250	This work

PDDA: poly(diallyldimethylammonium chloride); PG:porous graphene; GCE: glassy carbon electrode; UMP: uridine-5′-monophosphate; MPA: 3-mercaptopropionic acid; PPG: potentiostatically pretreated graphene; CNT: carbon nanotubes; RGO: reduced graphene oxide; GO: graphene oxide; 3D N-Co-CNT@NG: 3D nanocomposite of nitrogen doped Co-CNTs over graphene sheets; graphene/pectin-CuNPs: electrodeposition of copper nanoparticles(CuNPs) using biopolymer pectin as a scaffold and graphene as a support; Pt-IL-pGR-GCE: composite of Pt loaded on the support of porous graphene with ionic liquids; rGO/FeNPs nanocomposite: iron nanoparticles (FeNPs) decorated-reduced graphene oxide (rGO) nanocomposite; AuNPs@Gr/NiF: Au nanoparticles decorated graphene (AuNPs@Gr)/nickel foam (Gr/NiF) nanocomposite; CoWO4: $CoWO_4$ nanofibers (NFs) fabricated by using an electrospinning technique followed by high-temperature calcination.

sensors based on the reduction of hydrogen peroxide.

Acknowledgements

The authors thank CONICET (Nro. 11220150100710CO), PID SECyT-UNC (Res. 366/2016), ANPCyT (PICT 2016-1261), MINCyT-Córdoba (Resolución N° 000018/2014) for the financial support.

Appendix A. Supplementary data

Supplementary data to this article can be found online at https://doi.org/10.1016/j.microc.2018.05.019.

References

[1] W.W. Wang, Y. Qiu, S.P. Zhang, J.W. Li, X.-Q. Lu, X.H. Liu, Chin. J. Anal. Chem. 42 (2014) 835–841.
[2] X. Chen, B. Su, Z. Cai, X. Chen, M. Oyama, Sensors Actuators B 201 (2014) 286–292.
[3] E.W. Miller, B.C. Dickinson, C.J. Chang, Proc. Natl. Acad. Sci. U. S. A. 107 (2010) 15681–15687.
[4] C.C. Winterbourn, Nat. Chem. Biol. 4 (2008) 278–286.
[5] T.J. Preston, W.J. Muller, G. Singh, J. Biol. Chem. 276 (2001) 9558–9564.
[6] W. Chen, S. Cai, Q.Q. Ren, W. Wen, Y.D. Zhao, Analyst 137 (2012) 49–58.
[7] C.R. Holkar, A.J. Jadhav, D.V. Pinjari, N.M. Mahamuni, A.B. Pandit, J. Environ. Manag. 182 (2016) 351–366.
[8] J.N. Tiwari, V. Vij, C. Kemp, K.S. Kim, ACS Nano 10 (2016) 46–80.
[9] F. Mollarasouli, K. Asadpour-Zeynali, S. Campuzano, P. Yáñez-Sedeño, J.M. Pingarrón, Electrochim. Acta 246 (2017) 303–314.
[10] M.B. Gholivand, M. Khodadadian, Biosens. Bioelectron. 53 (2014) 472–478.
[11] J.H. Wang, X.J. Zhao, J.F. Li, X. Kuang, Y.Q. Fan, C. Wei, Z.Q. Su, ACS Macro Lett. 3 (2014) 529–533.
[12] M. Eguílaz, A. Gutierrez, G.A. Rivas, Sensors Actuators B Chem. 216 (2016) 629–637.
[13] G. Maduraiveeran, M. Sasidharan, V. Ganesan, Biosens. Bioelectron. 103 (2018) 113–129.
[14] C. Revathi, R.T.R. Kumar, Electroanalysis 29 (2017) 1481–1489.
[15] H. Wang, H. Wang, T. Li, J. Ma, K. Li, X. Zuo, Sensors Actuators B Chem. 239 (2017) 1205–1212.
[16] M. Somasundrum, K. Kirtikara, M. Tanticharoen, Anal. Chim. Acta 319 (1996) 59–70.
[17] H. Sakslund, J. Wang, O. Hammerich, J. Electroanal. Chem. 402 (1996) 149–160.
[18] J. Wang, J. Liu, L. Chen, F. Lu, Anal. Chem. 66 (1994) 3600–3603.
[19] J. Wang, G. Rivas, M. Chicharro, Electroanalysis 8 (1996) 434–437.
[20] M.S. Celej, G.A. Rivas, Electroanalysis 10 (1998) 771–775.
[21] M.C. Rodríguez, G.A. Rivas, Electroanalysis 13 (2001) 1179–1184.
[22] J. Liu, F. Lu, J. Wang, Electrochem. Commun. 1 (1999) 341–344.
[23] S. Miscoria, G. Barrera, G. Rivas, Electroanalysis 14 (2002) 981.
[24] S.A. Miscoria, G.D. Barrera, G.A. Rivas, Electroanalysis 17 (2005) 1578–1582.
[25] S.A. Miscoria, G.D. Barrera, G.A. Rivas, Sensors Actuators B 115 (2006) 205–211.
[26] G.L. Luque, M.C. Rodríguez, G.A. Rivas, Talanta 66 (2005) 467–471.
[27] L. Zhang, H. Li, Y. Ni, J. Li, K. Liao, G. Zhao, Electrochem. Commun. 11 (2009) 812–815.
[28] N.W. Beyene, P. Kotzian, K. Schachl, H. Alemu, E. Turkusic, A. Copra, H. Mderegger, I. Svancara, K. Vytras, K. Kalcher, Talanta 64 (2004) 1151–1159.
[29] E. Turkusic, J. Kalcher, E. Kahrovic, N.W. Beyene, H. Moderegger, E. Sofic, S. Begie, K. Kalcher, Talanta 65 (2005) 559–564.
[30] G.L. Luque, N.F. Ferreyra, G. Leyva, G.A. Rivas, Sensors Actuators B 142 (2009) 331–336.
[31] M.-P. Pileni, Adv. Funct. Mater. 11 (2001) 323–336.
[32] R. Zhang, W. Chen, Biosens. Bioelectron. 89 (2017) 249–268.
[33] Y. Su, H. Guo, Z. Wang, Y. Long, W. Li, Y. Tu, Sensors and Actuators B 255 (2018) 2510–2519.
[34] T. Dayakar, K. Venkateswara Rao, M. Vinodkumar, K. Bikshalu, B. Chakradhar, K. Ramachandra Rao, Appl. Surf. Sci. 435 (2018) 216–224.
[35] J.M. Sieben, A.E. Alvarez, V. Comignani, M.M.E. Duarte, Int. J. Hydrog. Energy 39 (2014) 11547–11556.
[36] A.R. West, Solid State Chemistry and its Applications, second ed., John Wiley & Son Inc., UK, 2014.
[37] T. Cochell, A. Manthiram, Langmuir 28 (2012) 1579–1587.
[38] T. Shibata, B.A. Bunker, Z. Zhang, D. Meisel, C.F. Vardeman, J.D. Gezelter, J. Am. Chem. Soc. 124 (2002) 11989–11996.
[39] H.M. Rietveld, J. Appl. Crystallogr. 2 (1969) 65–71.
[40] Y.W. Ma, H.M. Zhang, H.X. Zhong, T. Xu, H. Jin, X.Y. Geng, Catal. Commun. 11 (2010) 434–437.
[41] Y.C. Zhao, X.L. Yang, J.N. Tian, F.Y. Wang, L.Z. Zhao, Int. J. Hydrog. Energy 35 (2010) 3249–3257.
[42] W. Xue, X. Bo, M. Zhou, L. Guo, J. Electroanal. Chem. 781 (2016) 204–211.
[43] J. Liu, X. Bo, Z. Zhao, L. Guo, Biosens. Bioelectron. 74 (2015) 71–77.
[44] J. Liu, M. Zhang, J. Liu, J. Zheng, Anal. Methods 8 (2016) 1084–1090.
[45] X. Yang, Y. Wang, Y. Liu, X. Jian, Electrochim. Acta 108 (2013) 39–44.
[46] J. Balamurugan, T.D. Thanh, G. Karthikeyan, N.H. Kim, J.H. Lee, Biosens. Bioelectron. 89 (2017) 970–977.
[47] O.G. Sahin, Electrochim. Acta 180 (2015) 873–878.
[48] H. Zhang, X. Bo, L. Guo, Electrochim. Acta 201 (2016) 117–124.
[49] H. Yang, Z. Wang, C. Li, C. Xu, J. Colloid Interface Sci. 491 (2017) 321–328.
[50] X. Wang, X. Guo, J. Chen, C. Ge, H. Zhang, Y. Liu, L. Zhao, Y. Zhang, Z. Wang, L. Sun, J. Mater. Sci. Technol. 33 (2017) 246–250.
[51] S.-H. Liao, S.-Y. Lu, S.-J. Bao, Y.-N. Yu, L. Yu, ChemElectroChem 2 (2015) 2061–2070.

[52] A. Benvidi, M.T. Nafar, S. Jahanbani, M.D. Tezerjani, M. Rezaeinasab, S. Dalirnasab, Mater. Sci. Eng. C 75 (2017) 1435–1447.
[53] X. Lu, X. Xiao, Z. Li, F. Xu, H. Tan, L. Sun, L. Wang, Anal. Methods 6 (2014) 235–241.
[54] S. Dong, Q. Yang, L. Peng, Y. Fang, T. Huang, Sensors Actuators B 232 (2016) 375–382.
[55] V. Mani, R. Devasenathipathy, S.-M. Chen, S.-F. Wang, P. Devi, Y. Tai, Electrochim. Acta 176 (2015) 804–810.
[56] W. Zhao, J. Jin, H. Wu, S. Wang, C. Feng, S. Yang, Y. Ding, Mater. Sci. Eng. C 78 (2017) 185–190.
[57] Adel A. Abdelwahab, Electroanalysis 28 (2016) 1–7.
[58] C. Zhang, Y. Zhang, X. Du, Y. Chen, W. Dong, B. Han, Q. Chen, Talanta 159 (2016) 280–286.
[59] Y. Zhang, Y. Li, Y. Jiang, Y. Li, S. Li, Appl. Surf. Sci. 378 (2016) 375–383.
[60] X.-R. Li, M.-C. Xu, H.-Y. Chen, J.-J. Xu, J. Mater. Chem. B 3 (2015) 4355–4362.
[61] B. Amanulla, S. Palanisamy, S.-M. Chen, V. Velusamy, T.-W. Chiu, T.-W. Chen, S.K. Ramaraj, J. Colloid Interface Sci. 487 (2017) 370–377.
[62] Y.-M. Huang, H.-L. Zhang, A.-M. Yu, Y. Liu, Y.-W. Wu, Sens. Lett. 8 (2010) 864–870.
[63] L.A. Mercante, M.H.M. Facure, R.C. Sanfelice, F.L. Migliorini, L.H.C. Mattoso, D.S. Correa, Appl. Surf. Sci. 407 (2017) 162–170.
[64] C.H. Díaz Nieto, A.M. Granero, J.C. Lopez, G.D. Pierini, G.J. Levin, H. Fernández, M.A. Zon, Sensors Actuators B 263 (2018) 377–386.
[65] Z. Dena, Y. Gong, Y. Luo, Y. Tian, Biosens. Bioelectron. 24 (2009) 2465–2469.
[66] V. Mani, M. Govindasamy, S.-M. Chen, T.-W. Chen, A.S. Kumar, S.-T. Huang, Sci. Rep. 7 (2017) 11910, http://dx.doi.org/10.1038/s41598-017-12050-x.
[67] F.N. Comba, F. Gutiérrez, P. Herrasti, M.D. Rubianes, G.A. Rivas, Electroanalysis 24 (2012) 1541–1546.